The influence of dihedral bulbous bows on the resistance of small fishing vessels: a numerical study

H.R. Díaz-Ojeda[a,*], F. Pérez-Arribas[b], Stephen R. Turnock[c]

[a] *Instituto Universitario de Sistemas Inteligentes y Aplicaciones Numéricas en Ingeniería, Universidad de Las Palmas de Gran Canaria (ULPGC), Las Palmas de Gran Canaria 35017, Spain*
[b] *Universidad Politécnica de Madrid. (UPM), Calle Ramiro de Maeztu 7, 28040, Madrid, España*
[c] *Fluid Structure Interactions Group, University of Southampton, Boldrewood Innovation Campus, SO16 7QF, United Kingdom*

Abstract

Environmental aspects in the shipping industry are nowadays taking more relevance. Independently of the type of fuel used, good drawing lines in ships might help with the emission mitigation and also with the ship efficiency. In the fishing industry, ships lines in non-developed countries and in small traditional ships are normally not optimized what leads to a no optimal use of the resources and operation. In this work this topic is treated. The lines of two fishing vessels are studied numerically and compared with towing tank experiments. Those lines from a displacement and a semi-displacement hull, are optimized by adding a new type of bow named as dihedral bulbous bow. This bow produces a reduction over 10% of the ship's resistance. This work focuses on explaining numerically why that difference occurs. The bulbous bow reduces the pressure resistance by softening the flow that reaches the bow.

Keywords: Dihedral bow, Small fishing vessels, Computational fluid dynamics, Ship energy efficiency , OpenFOAM.

*Corresponding author
Email addresses: hectorruben.diaz@ulpgc.es (H.R. Díaz-Ojeda), francisco.perez.arribas@upm.es (F. Pérez-Arribas), S.R.Turnock@soton.ac.uk (Stephen R. Turnock)

Nomenclature

List of variables:

L Ship total length (m)

B Ship beam (m)

D Ship depth (m)

∇ Volumetric displacement of ship (m^3)

S Wetted surface area (m^2)

C_B Block coefficient

λ Scale

C_P Prismatic coefficient

Fr Froude number ($Fr = V/\sqrt{gL}$)

g gravitational constant(m/s^2)

$\triangle t$ Time step (s)

R_t Total resistance (N)

R_v Viscous resistance (N)

R_t Pressure resistance (N)

C_p Pressure coefficient

1. Introduction

The assessment of ship resistance in calm water is normally one of the most relevant factors when a new ship design is proposed. This factor affects a large number of areas that need to be taken into account in the design process. For instance, the engine power and size, ship emissions or propellers election. An over or under of power estimations may well change the economic effectiveness of the ship. The velocity - resistance curve needs to be determined for any hull shape at its service conditions to a high degree of accuracy. When a comparison of ship hulls is proposed, the resistance will determine which hull shape is more efficient or which bow configuration is better in hydrodynamics terms.

Typical fishing vessels have a number of service speeds from transit to the fishing grounds, searching for fish, fishing itself, to return to port with a valuable cargo always taking into account the restrictive environmental regulations in terms of power options for reducing its environmental impact Korican et al. (2022). In comparing alternate hull designs, the resistance for each service speed and associated load condition will need to be considered. Bulbous bows have been found to help reduce resistance by altering the effective vessel length and reducing its wave pattern resistance. However, such designs have often been optimised for just one service and load condition. The application of bulbous bows to fishing vessels has previously been considered to be too expensive both in design and in a production cost

to be considered.

The cost of a bulbous bow can be reduced if developable surfaces are used, like in the dihedral bows studied in this paper. The full design process is presented in Pérez-Arribas et al. (2022), and the final result are a set of developable surfaces as presented in figure 1 right. The design of a dihedral bow considers a set of 3D lines that are used as boundaries for the developable surfaces, and that are integrated into the original hull, as the lines T, C and K presented in figure 1 left.

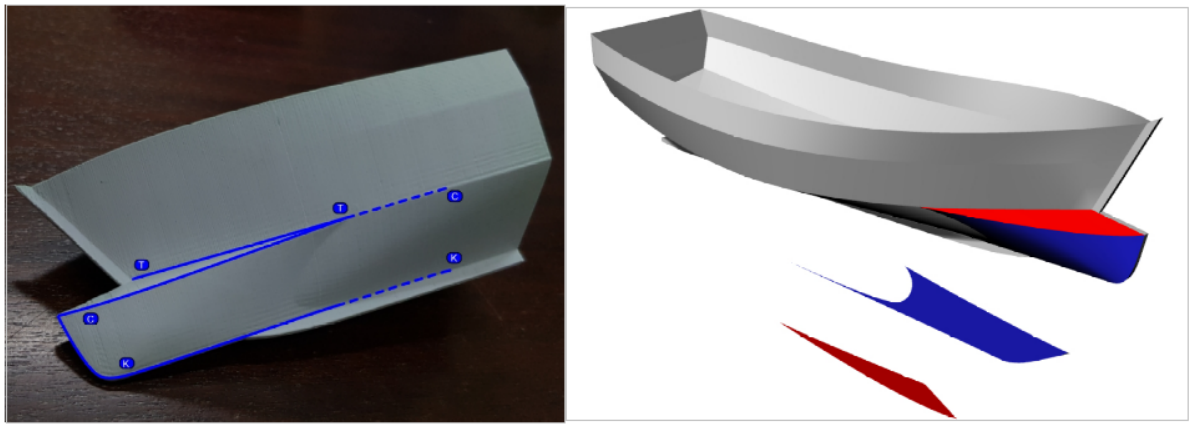

Figure 1: Dihedral bulbous bow design

The main novelty of this bulbous bow design was the use of developable surfaces, and the design produces an important reduction into the ship's resistance over 15% for some speeds as presented in Pérez-Arribas et al. (2022), were two different ships were studied experimentally.

Historically, the ship powering have been predicted with statistical regressions or experimentally Molland et al. (2017) . Statistical regressions of the model test, for instance Holtrop and Mennen (1982) or Guldhammer and Harvard (1974), are nowadays used as an 'early design tool'. There are a large number of statistical methods with limitations in Froude range, type of vessel, or ship shape for instance. Those methods are created based on towing tank tests and in some cases, they include correlation with sea trial tests. The uncertainty created by those methods can be appreciated if the resistance obtained by those methods is compared with experimental tests when a new design is studied. Is difficult to

quantify the effect of local modifications in the ship hull, i.e. different bows, rudder or ship lines, due to their statistical character.

Experimental techniques have been used with a high level of accuracy not only for creating the statistical methods but also as a tool in the design stage of the protect. Towing tank experiments give the chance of testing new concepts like those proposed by Yanuar and Waskito (2017) where the total hull resistance of a pentamaran is evaluated and no statistical method can be used. Experimental test are generally expensive and limited by the availability of a towing tank. In addiction, the construction of the experimental model makes the tests campaign longer in comparison with a statistical method.

Nowadays, the fast development of computers and technology introduces the possibility of using numerical tools for determining the ship velocity - resistance curve. The ITTC (International Towing Tank Conference) benchmarking run since 1980 Larsson et al. (2015), ITTC (2021) have quantified the progress in the improvements in accuracy, the influence of mesh size and turbulence model as well as sophistication of the simulations. Calm water resistance CFD can be expected to be with low error compared with the model resistance and able to distinguish between local hull features at an even higher level of accuracy.

Some examples of the use of CFD simulations ,Voxakis (2012) simulated a destroyer hull against experiments, Niklas and Pruszko (2019) proposed computational fluid dynamics (CFD) as an feasible alternative method to towing tank, Szelangiewicz et al. (2021) study the effect of adding a bulbous bow to a small fishing vessel and Sugianto et al. (2022) evaluates the effect of a monohull in comparison with a catamaran hull using OpenFOAM.

CFD have been proven as an efficient and reliable tool in fluid dynamics also obtaining the wake of other marine structures like the comparison done by Díaz-Ojeda et al. (2019) against experimental particle velocimetry in terms of the vorticity field or Rabaud and Moisy (2013) that used numerical wake patterns for comparing the Kelvin and Mach angle. For those reasons and also because most of the numerical studies include data that are difficult to obtain experimentally like pressure fields, numerical analysis is a very interesting alternative when ship hydrodynamics needs to be evaluated.

When CFD is used, best practice guidelines should be followed (ITTC (2008), ITTC

(2011), ITTC (2014), ITTC (2017b)). Those guidelines help to reduce the uncertainty created by the CFD. Those guidelines should be used together with research papers like Islam and Guedes Soares (2019) where the well known models KCS, DTC KVLCC2 and JBC are studied providing a valuable information about the numerical procedure. This research shows that although the different hulls simulated have similarities, mesh dependency for each hull is different and therefore each case should be treated independently. Another important issue when ship resistance is calculated using CFD is the turbulence modelization. The review done by Pena and Huang (2021) deal with the different turbulence models and simulations. As summary, it indicates that the Reynolds Average Navier-Stokes equations are a good approach when a turbulence strategy is followed for ship hydrodynamic simulations with a relatively low computational cost. Finally, some recommendations about the mesh and time step sensitivity should be considered due to the crucial role that plays in CFD simulations Jasak et al. (2013), Jasak et al. (2019).

Before using the procedures introduced before, optimizations or new designs needs to be developed. Most of the hull optimizations use the CFD as a comparison tool of the quality of the design in terms of resistance. Xu and Wang (2001) proposes an optimization procedure based in 5 levels. The results from the model created by following this process show that CFD is a good approach that helps in the hull optimization since the resistance performance can be compared feasibly. Kim and Yang (2010) develop a surface modification for CFD-based ship form optimization. In this study done in the classical KRISO container ship and the KCS show a drag reduction when this methodology is applied.

Many optimization studies focus on the bulb of the ship as an essential method for drag reduction, Campana et al. (2006), Percival et al. (2001), Zha et al. (2021) Huang and Yang (2016), Liu et al. (2021) and Nazemian and Ghadimi (2021). All of whom use multi-objective optimization to find the optimal shape. Based on this interest, in this work dihedral bulbous bow, are studied in order to evaluate its efficiency in terms of resistance in calm water.

A dihedral bulbous bow is a type of developable bulbous bow that is quite similar to the beak bow that is present in some large ships but as main difference, a dihedral one is piercing the water surface and not fully submerged. A dihedral bulbous bow has marked

chine lines, making this developable bow easier to manufacture and enabling the retrofitting of designs without a bulbous bow. The chine lines also define the hydrodynamic behaviour of the design.

The shape of a dihedral bow is quite distinctive and can be designed well integrated into the original design, or as an addition to the hull as it is presented in the present paper. A good design of a dihedral bow with a balanced design of the hull and position of the center of gravity can produce a very good boat when compared with a ship without a bulbous bow. The dihedral bow of this papers show resistance reductions with original hulls next to a 20%.

This paper studies numerically the new type of bow introduced before, the dihedral bow, Pérez-Arribas et al. (2022). The proposed dihedral bow is going to be implemented in a model provided by the fishing vessel design database (FVDD) of FAO (Food and Agriculture Organization of the United Nations) FVDD (2021). This data base provide detailed lines drawings of fishing vessels prepared by FAO and other naval architects with the purpose of being used for research, use, replication and modification.

Generally, the effect of bulbous in smaller ships has had limited investigation. In this work the effect of dihedral bow in a small fishing vessel is analysed. The research will be carried out with the numerical open source OpenFOAM. The installation of such a bow shape can reduce the ship resistance over 10 %, with significant saving in fuel consumption Pérez-Arribas et al. (2022). After a validation with experiments, pressure field and wave analysis are presented to explain the hydrodynamic effect of the dihedral bow.

This paper is divided as follows: First, a problem description will be shown in section 2 where an introduction of the towing tank experiments and CFD is done. Then, in section 3 a description of the numerical methods, the mesh description and the experimental methodology is presented. In section 4 a numerical validation is done against the experimental results. Then, in section 5 the bow analysis is done presenting a conclusion in section 6. Finally, references are presented in the latest section.

2. Problem description

2.1. Introduction

The investigation starts with towing tank experiments where drag forces were obtained and evaluated for different ship shapes and velocities, and presented in Pérez-Arribas et al. (2022). Subsequently, the same cases were simulated numerically serving the experimental results as a validation. The numerical simulations will add extra data that cannot be obtained experimentally such as pressure field and force decomposition. The study will be carried out at a ship model of scale $\lambda = 4$. The different velocities evaluated in this research are $1.029, 1.286, 1.543$ and $1.8 m/s$. This leads, to Froude numbers between 0.21 and 0.38.

2.2. Hull form

Two different hull shapes are used for the current study. Figure 2 and 3 shows in yellow the original models from FAO and in red the cases with dihedral bows that are going to be compared.

For figure 2, the hulls are named FAO1 for the yellow one and FAO1b for the bulbous one. Similarly, in figure 3 the yellow hull is named FAO2 and the red one FAO2b. The details about dimensions and their main characteristics are provided in table 1. Both ships were designed to operate as short distance fishing vessels in the coasts of Nigeria and Virgin Islands since FAO promotes the local fisheries in developing countries.

Ship	λ	$L(m)$	$B(m)$	$D(m)$	$\nabla(m^3)$	$S(m^2)$	C_B	C_P
FAO1	4	2.308	0.751	0.643	0.098	1.5	0.284	0.597
FAO1b	4	2.308	0.751	0.643	0.103	1.588	0.275	0.578
FAO2	4	1.893	0.741	0.564	0.084	1.346	0.262	0.723
FAO2b	4	1.893	0.741	0.564	0.088	1.422	0.253	0.699

Table 1: Model characteristics

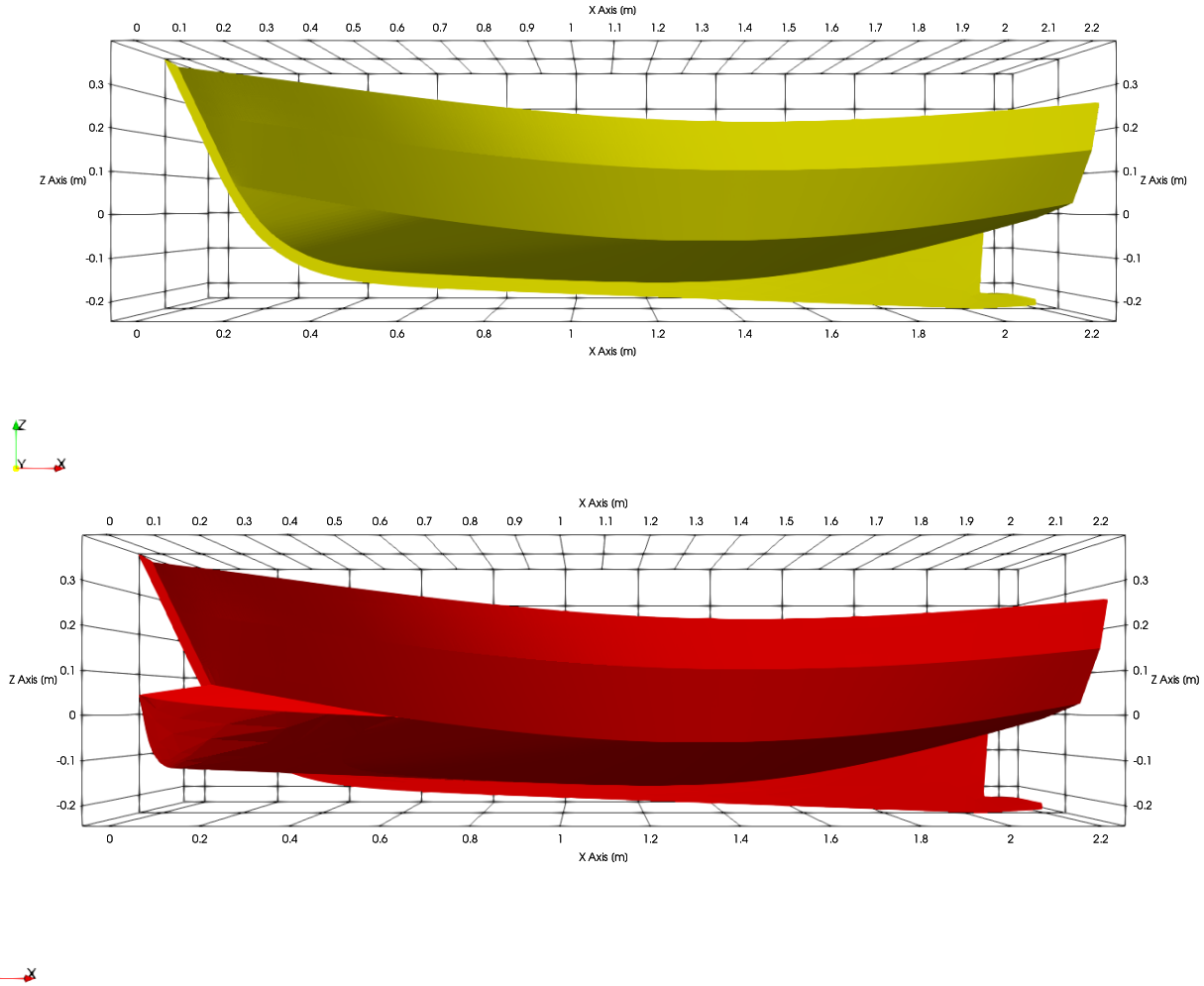

Figure 2: Yellow hull without polyhedral bulbous bow (FAO1). Red hull with polyhedral bulbous bow (FAO1b)

2.3. Towing tank tests

The experimental studies were carried out in the Naval School of the Technical University of Madrid (ETSIN) in a towing tank of 100 meters length, 3.8 meters breath and 2.2 meters depth (figure 4). A complete description of the experiments have been published in Pérez-Arribas et al. (2022).

Figure 4 presents the test set up scheme, where the model is connected to the towing carriage by two guide arms, a wire, a spring, and a force sensor. Before each run, the zero measurement of all sensors is taken. The waiting time between two consecutive tests was

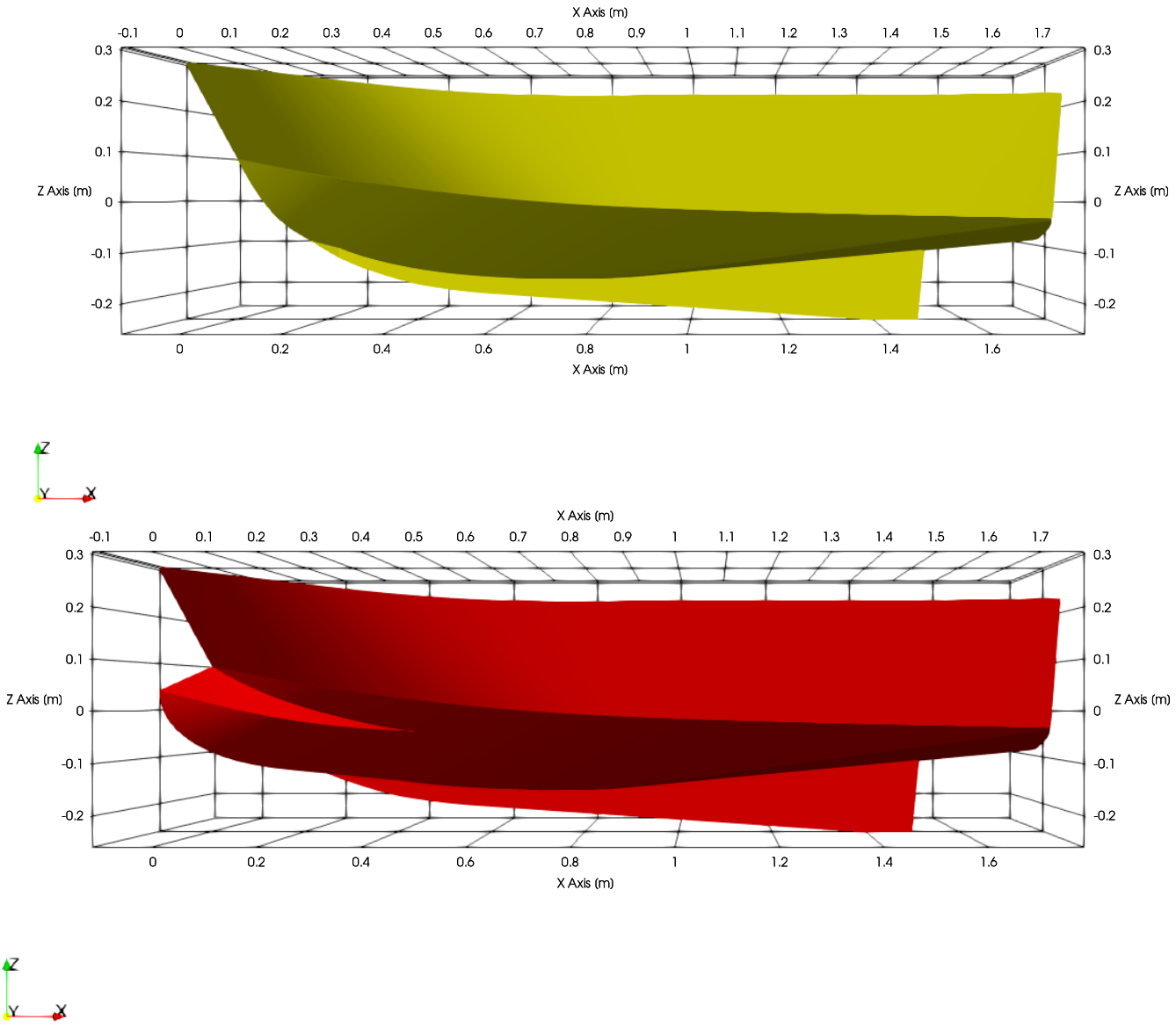

Figure 3: Yellow hull without polyhedral bulbous bow (FAO2). Red hull with polyhedral bulbous bow (FAO2b)

about 20 to 25 minutes in order to get a quiet water free surface. The water level of the basis was checked to maintain a constant value during all the experimental campaign.

Each run stars by accelerating the carriage up to the required speed, and in a similar fashion the numerical calculations are made. During the acceleration phase, the clamp of 4 restrain the model to avoid high stresses on the force sensor. The guiding arms permits the

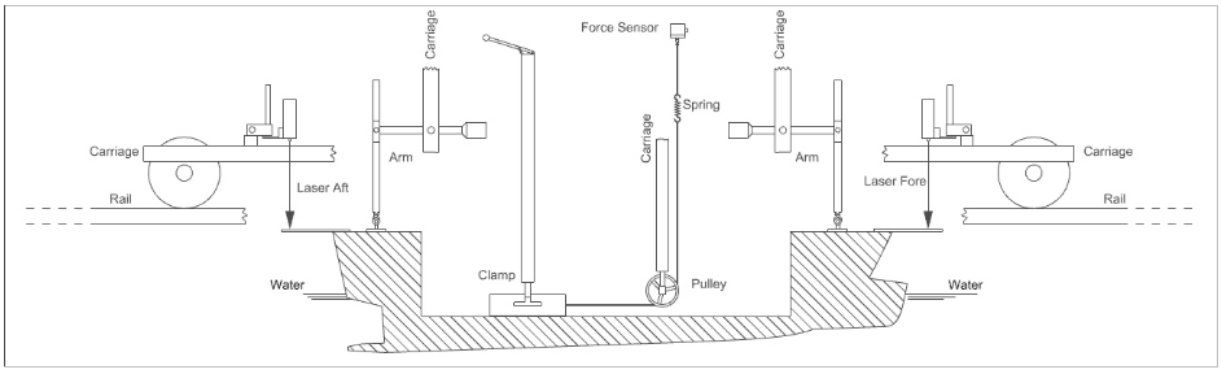

Figure 4: Transversal view of Tank at ETSIN and power test set up

model to move in pitch, heave, and surge, restraining the rest of motions. Two laser beams, placed fore and aft, allow the measurement of sink and trim of the model.

The towing resistance was measured with a strain sensor (Z6 bending beam dynamometer) directly joined to the carriage through a calibrated pulley, spring and wire system. The strain cell uses a sampling of 10 Hz for measuring the force that is parallel to the advance direction. The dynamometer was calibrated in a greater range than the maximum measured force, about 4 kg. Although the results presented in this paper are in model scale, the water temperature was measured to extrapolate the results to full scale at 16^oC following ITTC (2017a).

2.4. Computational simulations

The numerical studies were developed with the open source OpenFOAM version 7. OpenFOAM is an open source computational fluid dynamic package that is written in C++. This code, that implements the finite volume method, will compute the calm water resistance in the different cases using a symmetry boundary condition along the vertical centre line. Using this strategy, the mesh requirements are halved.

The domain is built in two parts, the top part that is filled with air and the bottom part that is filled with water. These two inmiscible fluids are present in this case together with the presence of free surface and gravity. The dimensions used for the computational domain are presented in table 2 where the forward perpendicular is considered the origin.

	E	$E1$	B	$H1$	A
$Distance$	16	4.6	4.90	7	4.6

Table 2: Domain dimensions in meters of 5

The computational domain used is presented in figure 5.

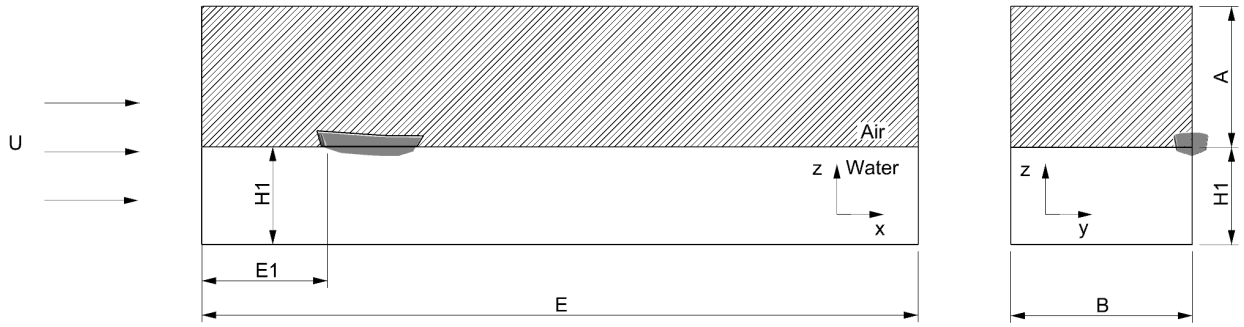

Figure 5: Problem set up and main parameters

The procedure for simulating each case is divided in two stages, see figure 6. In the first one, the ship is considered rigid and no sink or trim is allowed. In this first stage, the simulation is made once the flow and the forces converge. This takes a time of ten simulation seconds. The results from this first stage are not considered. A second step follows and the ship is allowed to move in heave and rotate in pitch (sink and trim). During this part of the simulation the force in x axis is is evaluated once the ship has its equilibrium position.

For all cases, after a time step and mesh convergence study, the the time step selected is $\delta t = 6 \times 10^{-4}$ and the mesh size is around 7.5 million cells that will be discussed in 4. The fluid flow comes uniformly in the x direction and the fluid properties are kept constant in all the simulations.

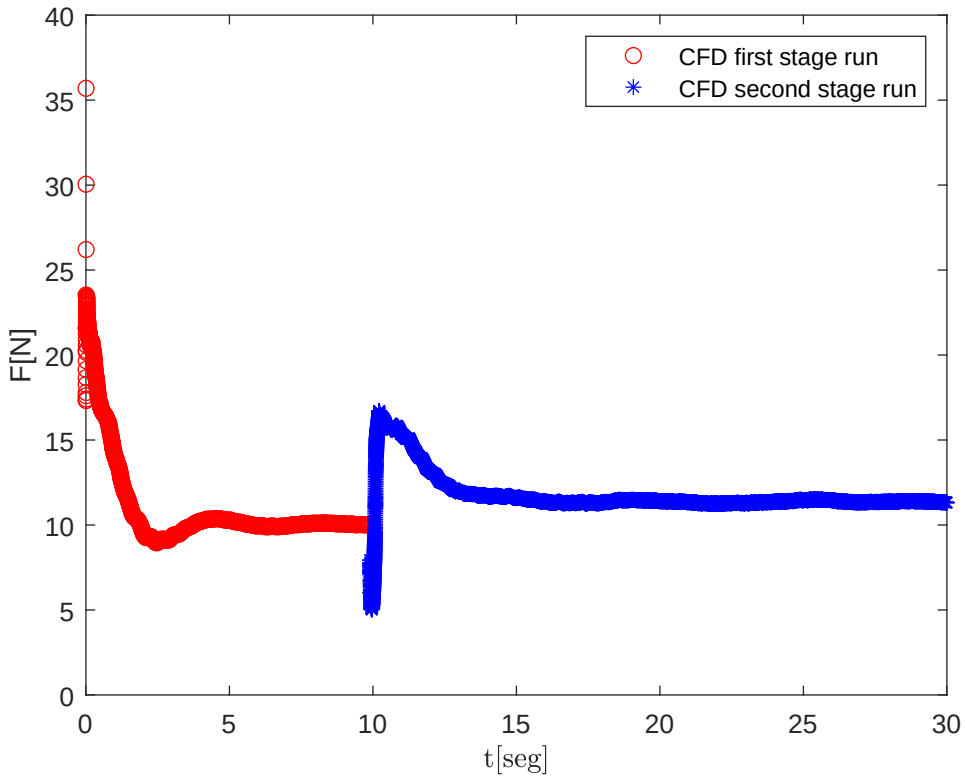

Figure 6: Drag forces for first and second simulation stages for FAO2b v = 1.286 m/s

3. Methodology

3.1. Numerical methods

In this section the relevant aspects of the numerical part are described. The set up and the case configuration is kept identical to all the simulations once it is validated with experiments. The numerical tool snappyHexMesh is used for the mesh creation which is included in OpenFOAM.

3.1.1. Fluid dynamics solver

The equations to be solved for the fluid part are the incompressible Navier-Stokes equations. The references for the fluid dynamics and the numerical schemes are Versteeg and Malalasekera (2007), Moukalled et al. (2015) and Oro (2012) where any concept that might be involved in this work can be consulted with more detail. The Reynolds number is moderate and turbulence flow is considered when a ship model is tested. Therefore, turbulence

is implicit in this work. According with Pena and Huang (2021), RANS models are a good option due to the prohibitive computational cost of Direct Numerical Simulation (DNS) and Large eddy simulation (LES). Although LES models could be used, comparing LES with Reynolds Average Navier Stokes (RANS) models, the last one can provide good force results if the numerical model and strategy is well selected with less computational cost. Therefore, for this study RANS model will be used. Therefore, the equations to be solved are the time averaged Navier - Stokes presented in section 3.1.1.

$$\nabla \cdot \overline{\mathbf{v}_f} = 0 \tag{1}$$

$$\frac{\partial(\rho_f \overline{\mathbf{v}_f})}{\partial t} + \nabla(\rho_f \overline{\mathbf{v}_f \mathbf{v}_f}) = \rho_f \mathbf{g} - \nabla \overline{p} + \mu_f \nabla^2 \overline{\mathbf{v}_f} \tag{2}$$

where $\overline{\mathbf{v}_f}$ is the fluid velocity vector, $\overline{p}$ is the time average pressure, ρ_f the fluid density and μ_f the fluid viscosity. Due to the presence of water and air, the viscosity change locally. OpenFOAM (OpenFOAM) implements a transient PISO algorithm (Pressure Implicit Splitting of Operators) Issa (1986) that solve the unsteady Navier Stokes equations. This algorithm implies two corrector steps and one predictor step being an extension of SIMPLE (Semi-Implicit Method for Pressure Linked Equations) algorithm but with an extra corrector step to enhance it.

For the discretization schemes, Euler scheme is used for time discretization and a second order upwind scheme was used for the convection term. In the case of the gradient discretization, the used scheme is the Gauss linear one. As well as for the Laplacian scheme where the discretization was done with Gauss linear corrected.

The turbulence model is the k-omega shear stress transport SST-Model (SST-Model) Menter (Menter) and Menter (1994). This model that is based on a two equation model for the turbulence kinetic energy k, and the turbulence specific dissipation rate ω. The model is able to capture flow separation being an enhanced version of the $K - \omega$ model Menter et al. (2003).

The Volume of Fluid method (VOF) determines the free surface when two immiscible

fluids are present. This method uses a scalar α defined on each cell whose value is zero when a fluid A fill the cell and it value is 1 when a fluid B fill the cell. For values between 0 and 1, both fluids are present in the cell proportionally sharing the cell. (3) is the equation used to model the volume fraction for one phase not taking into account mass sources or any mass transfers between phases.

$$\frac{\partial \alpha}{\partial t} + \mathbf{v} \cdot \nabla \alpha = 0 \tag{3}$$

When α is found, ρ_f and μ_f are computed accordingly for each cell. This method is used for solving the free surface interaction.

The boundary conditions used for this work are the inlet mean velocity $\overline{v}$ and fixed inlet flux pressure. For the hull, the boundary condition used is no slip for the velocity and zero normal gradient for the pressure. Zero gradient is used in velocity and pressure for outlet wall being symmetry plane condition for the wall that splits the hull and domain in two. Finally, the rest of the domain boundaries, top, back side, and bottom, are established as walls with slip condition.

3.1.2. Mesh description

The mesh structure is described in this subsection. The strategy followed is similar to the described in Sugianto et al. (2022). Different meshes and mesh structures were tested until a final mesh result was defined, see figure 7. The mesh validation is described in section 4.

The mesh is built into 6 blocks, $R1$, $R2$, $R3$, $R4$, $R5$ and $R6$. The initial position, $coordinate_{ini}$, and the end position, $coordinate_{end}$, of each block are shown in table 3.

Each box have an extra degree of refinement than the previous box. The cell refinement is bigger in the following order $R1 < R2 < R3 < R4 < R5$. Specific refinement for the interface is done in box $R6$. This one will help with the numerical convergence of the equations solved in the free surface and for a better resolution of the ship wake. Finally, an extra refinement is done in the boundary layer as can be appreciated in 7.

The mesh used for all the cases according with the validation 4 is $\sim$ 7,5 million cells.

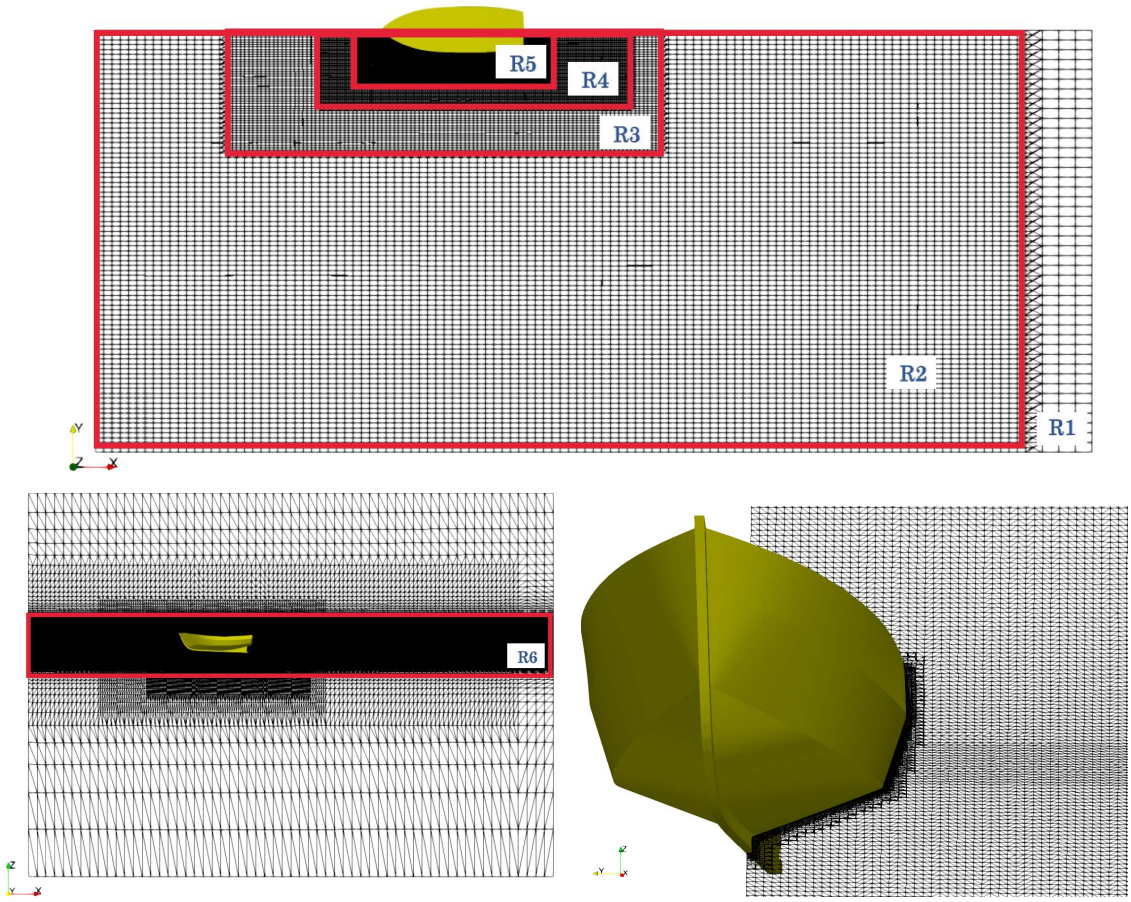

Figure 7: Top: mesh view for XY plane at Z=0. Bottom left: XZ plane at symmetry boundary. Bottom right: YZ plane at ship midship.

There is a small variation of the number of cells in each case due to the change in geometry by adding the dihedral bow.

3.2. Dimension parameters

In this work, different magnitudes and dimensionless parameters are used. The length L of the model will serve as characteristic length. Other magnitudes that take part in our problem are the fresh water density $\rho_f^b = 999.35 kg/m^3$ and cinematic viscosity $\mu_f^b = 1.145 \times 10^{-6} m^2/s$ for the bottom part of the domain, and for the top part of the domain the air density $\rho_f^a = 1 kg/m^3$ and cinematic viscosity $\mu_f^a = 1.48 \times 10^{-5} m^2/s$. The gravity acceleration g is considered to be fixed with a value of $9.81 m/s^2$.

	$\frac{x_{ini}}{L}$	$\frac{x_{end}}{L}$	$\frac{y_{ini}}{L}$	$\frac{y_{end}}{L}$	$\frac{z_{ini}}{L}$	$\frac{z_{end}}{L}$
R_1	-1.99	4.90	-2.92	0	-3.04	1.99
R_2	-1.99	4.90	-2.92	0	-1.19	1.06
R_3	-1.08	1.95	-0.87	0	-0.87	0.60
R_4	-0.43	1.73	-0.54	1.17	-0.69	0.43
R_5	-0.22	1.19	-0.39	0.69	-0.43	0.28
R_6	-1.99	4.90	-2.92	0	-0.33	3.33

Table 3: Mesh blocks dimension

4. CFD validation

Before analysing the data provided by the CFD about the influence of the dihedral bow, a validation is done. FAO1 and speed 1.543 m/s case is selected for validation. Different set ups, meshes and time steps were compared with the experimental resistance in order to reach a configuration that matches the results. In this section, we present the results that serve as proof of the numerical set up and configuration. Brevely, in table 4 the most relevant results are presented. In this table the the error is computed against the experimental result $(Experimental - Numerical/Experimental)$.

Case	$\triangle t$	Mesh cells	Fr	$F[N]$	Error (%)
Experimental FAO 1	-	-	0.33	15.31	-
Numerical FAO 1	6×10^{-5}	7552418	0.33	15.25	0.40
Numerical FAO 1	6×10^{-5}	5454540	0.33	15.72	2.7
Numerical FAO 1	4×10^{-5}	7552418	0.33	15.37	0.43

Table 4: FAO1 validation

In table 4 it is shown that agreement in terms of mesh size is fulfilled due to the low errors in comparison with the experimental data. In addition, the use of a smaller time step

does not show significant advantage or a large change in results. Therefore, this parameter is also validated. Besides, in figure 8 the pressure field is shown in the free surface with a good resolution due to the mesh, as it was studied in Islam and Guedes Soares (2019).

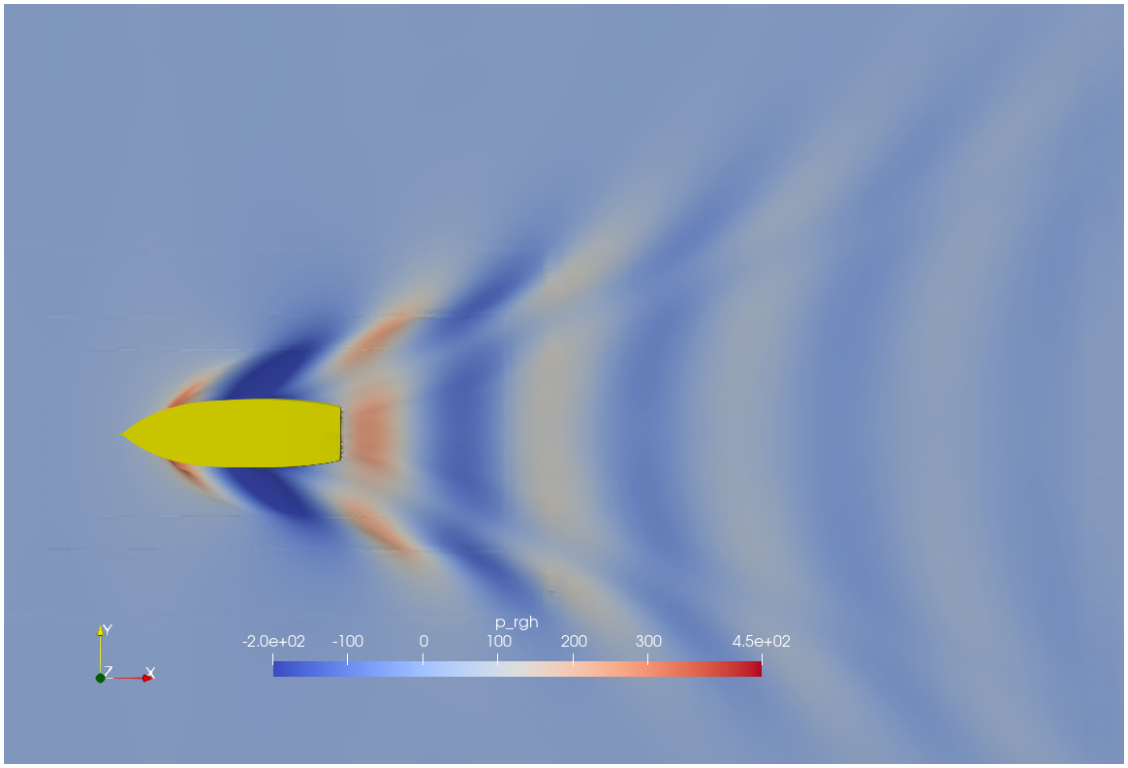

Figure 8: Free surface pressure distribution for FAO1, $v = 1.543 m/s$

Comparing wave pictures between experimental and numerical analysis, see figure 9, it can be appreciated that the CFD reproduces the wave generated for the FAO1 with similitude.

Finally, according to 4, for further studies the mesh size used will be the mesh with $\sim$ 7.5 million cells and the time step selected is 6×10^{-5}.

5. Results

In this section an analysis of the results is presented. The forces of the two cases, FAO1 and FAO2 are compared with the forces obtained for the cases FAO1b and FAO2b that include the dihedral bow. In figure 10, the experimental forces in Newtons for the

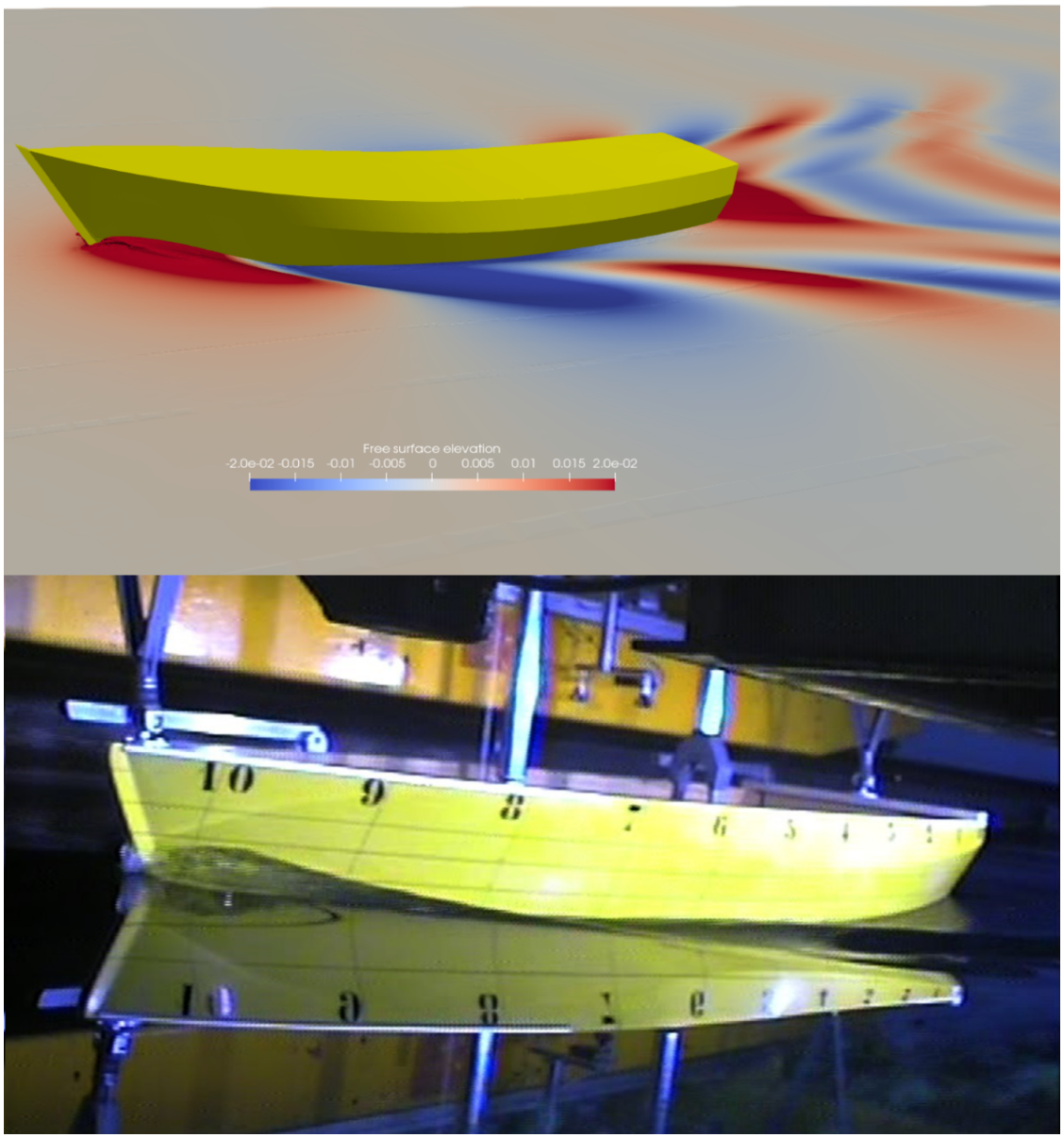

Figure 9: FAO1 v=1.543 m/s. Top CFD case. Bottom experimental case.

four models are plotted either numerical and experimental. The four velocities of study $v = [1.029, 1.286, 1.543, 1.8]$ m/s showed good agreement between the numerical simulations and the experimental towing tank tests. Those results verify the capability of the numerical studies for the resistance calculation. The results show less difference in total force with the experimental results for lower velocities. In order to quantify if the bigger error between numerical and experimental test is due to mesh or time step, since the convergence was only

made for $v = 1.543m/s$ and FAO1, a different hull shape, case FAO2 and v = 1.8 m/s, is selected and analysed. A new convergence analysis for a 12 million cells mesh and 4×10^{-5} seconds time step was performed for FAO2 obtaining the same error between numerical and experimental results. This might indicate that the difference should be due to numerical errors in the schemes, turbulence or even because the uncertainty in the experimental results.

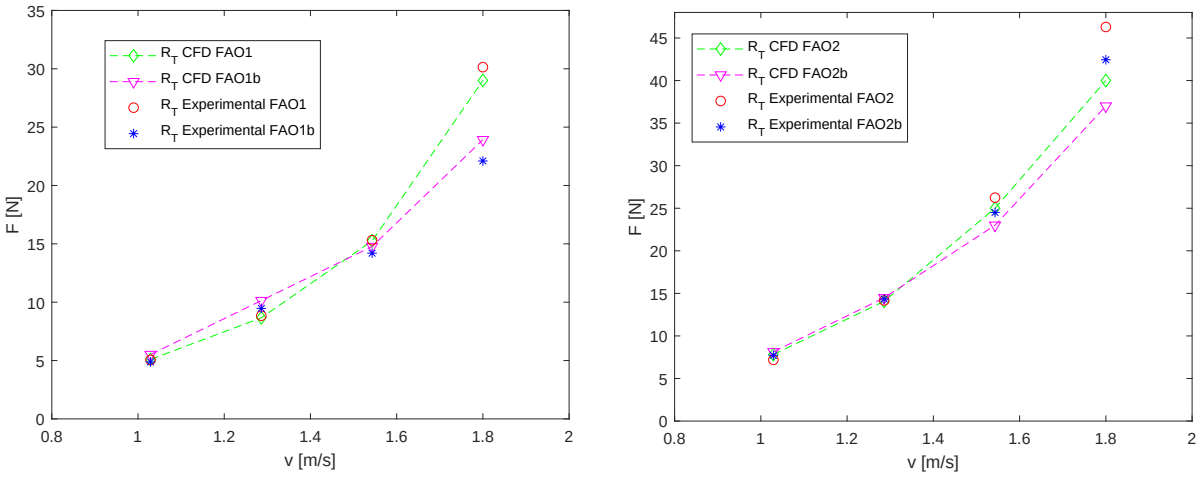

Figure 10: Total resistance against velocity for FAO1 and FAO1b(left) and FAO2 and FAO2b (right)

Once it is clear that the CFD results can be trusted for the different velocities as it was presented in figure 10, an explanation from the improvement in resistance due to the dihedral bow is treated. To distinguish what force is dominant in the problem, a resistance decomposition is done. Therefore, the resistance will be divided in two, viscous resistance $[R_v]$ and pressure force $[R_p]$. This division is presented only numerically.

In figure 11 the viscous force result for the different cases and velocities is presented. For FAO1 and FAO1b the viscous resistance for lower velocities, $v < 1.543$ m/s, seems not have significant difference if the dihedral bow is used. For $v = 1.8$ m/s there is a difference in the viscous resistance being larger for the FAO1b. This difference in the R_v only occurs for FAO1 at v = 1.8 m/s insomuch as FAO2 and FAO2b the R_v is similar for the whole range of speeds. This should be related with the bigger displacement of FAO1/FAO1b in comparison with FAO2/FAO2b where the R_v is close. This bigger displacement and the use of higher speeds might add extra frictional resistance.

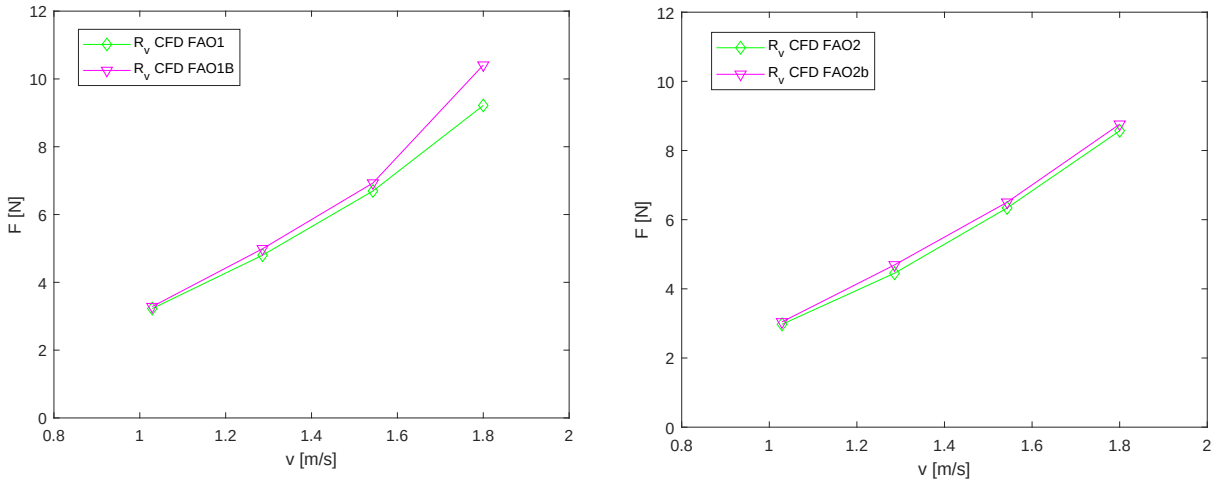

Figure 11: Viscous resistance against velocity for FAO1 and FAO1b(left) and FAO2 and FAO2b (right)

According with figure 11 no significant enhancement is produced by the use of the dihedral bow if only R_v is taken into account. However, in figure 12, where the pressure resistance $[R_p]$ is presented, the results show a different history. For FAO1 and FAO1b, it can be appreciated that the biggest difference in R_p is for $v = 1.8$ m/s. For this velocity, the R_p is larger for the case without bow, FAO1, in contrast with it was happening for the R_v, fig 11, where the R_v was larger for the case with polyhedral bow, FAO1b. According with this result, the dihedral bow in this case softens the incident flow making a reduction in R_p. Although, this flow , v= 1.80 m/s for FAO1/FAO1b, produces a larger R_v, in average R_p seems to be determinant for this case. Therefore, there is a substantial improvement when the dihedral bow is used due to the reduction of pressure resistance.

For lower velocities, $v < 1.543$ m/s, there is not a clear tendency in R_p that indicates an improvement in the total resistance if the dihedral bow is used. The difference in R_p is not as evident for the speeds $v = 1.543$ and $v = 1.029$ m/s, while for $v = 1.286$ the use of polyhedral bows produce a higher value of R_p. Those results indicates that the optimum working point for polyhedral bow in FAO1/FAO1b, that is a displacement hull, is with higher velocities.

For FAO2 and FAO2b, that is a semi-displacement hull, the R_p is identical for $v < 1.286$ m/s. This result, together with the result provided by the R_v notice that there is no

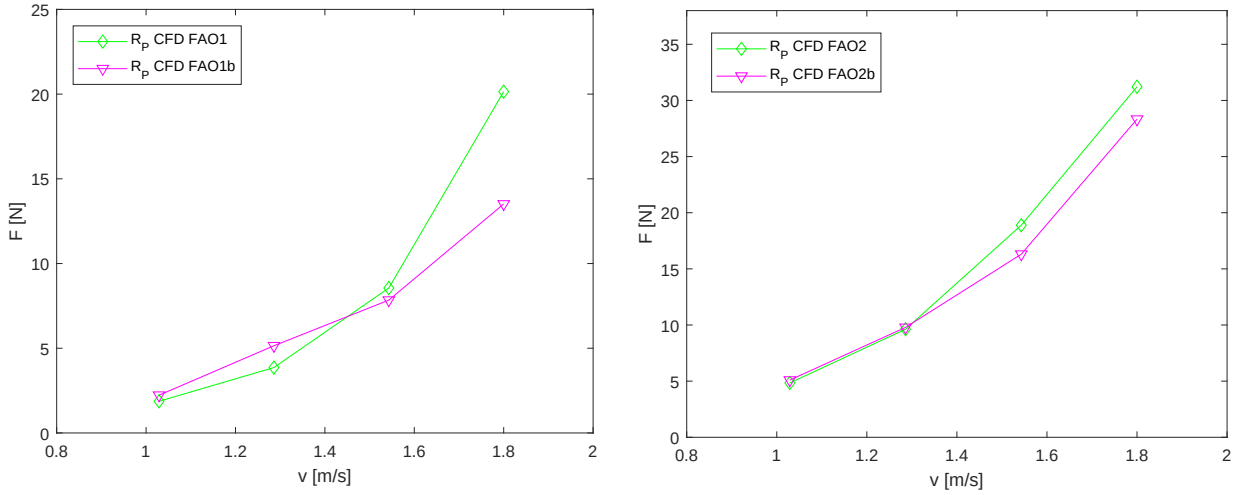

Figure 12: Pressure resistance against velocity for FAO1 and FAO1b(left) and FAO2 and FAO2b (right)

improvement in the use of the bow for those conditions. For larger velocities, $v \geq 1.543$ m/s, the pressure resistance is different and bigger for the case without bulbous bow. In this case the difference is not as pronounced as in FAO1/FAO1b because FAO2/FAO2b are semi-displacement hulls and they seem not to be as much affected by fluid pressure force as FAO1/FAO1b . Nonetheless, in average, there is a reduction in total resistance if the polyhedral bow is used for FAO2/FAO2b and speeds $v \geq 1.543$ m/s. This can be appreciated in figure 13 where total forces and forces decomposed are presented numerically together with the experimental results.

Figure 13, reveals that the most relevant proportion of forces in the total one comes from the R_p. For FAO1 and FAO1b and $v < 1.543$ m/s, the forces proportion between R_v and R_p seem to be close while for $v = 1.8$ m/s R_p is substantially higher.

R_v for FAO1 and FAO1b becomes more relevant for lower velocities due to viscous effects. The grow of the viscous resistance is linear. When R_p is analyzed for FAO1, the linear growth of R_p is not present meanwhile for FAO1b it exist. Therefore the dihedral bow breaks the critical point in R_p making pressure resistance grow linearly for v = 1.543. The critical point that might be located between v = 1.286 m/s and v=1.543 m/s is the point where R_p grows exponentially.

For FAO2 and FAO2b, the trend in R_v is also linear as it was in FAO1 and FAO1b.

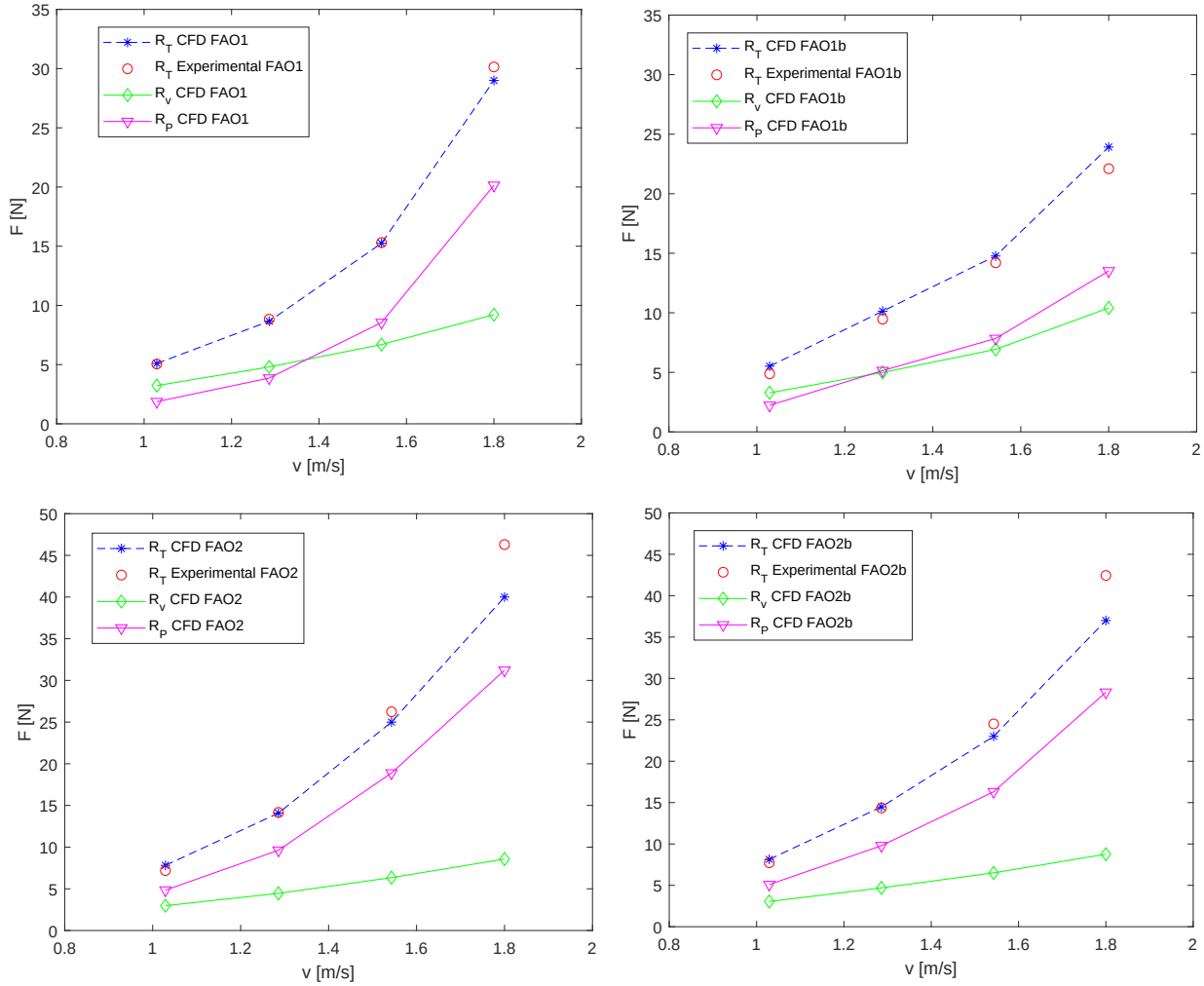

Figure 13: Total resistance and resistance decomposition

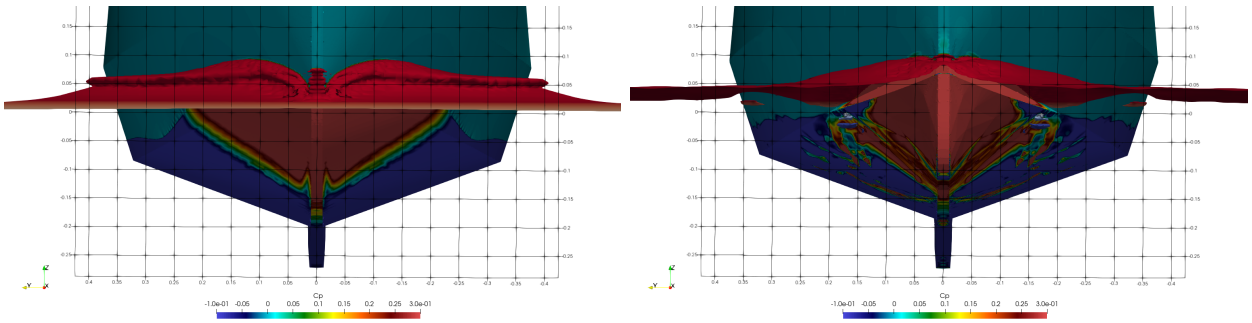

Figure 14: C_p at 1.8 m/s for: FAO1 left , FAO1b right expressed in a $y-z$ plane with subdivisions in meters of 0.05 by 0.05.

The R_p slope is most pronounced for FAO2 being slightly less pronounced for FAO2b. In this case, the pressure is also the determinant resistance and it is what the bow flow is changing substantially. The difference between FAO1/FAO1b and FAO2/FAO2b is mainly the displacement. Therefore, according with this results the polyhedral bow works better when the hull, has more displacement and larger speeds.

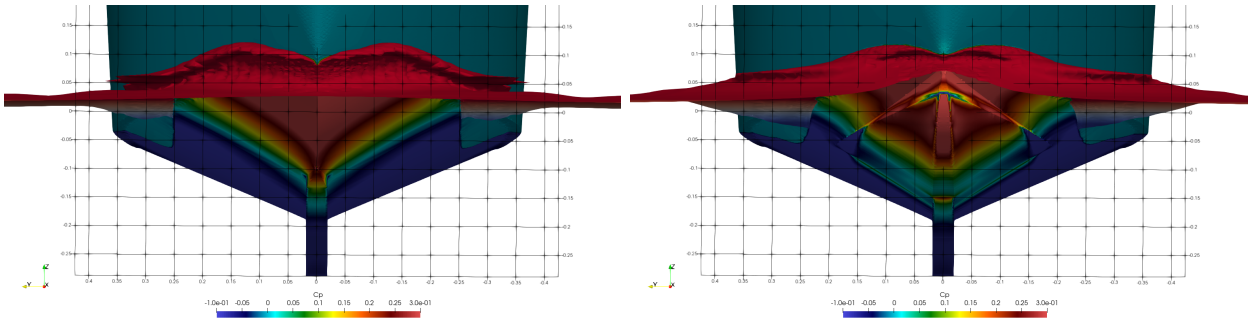

Figure 15: C_p at 1.8 m/s for: FAO2 left and FAO2b right expressed in a $y-z$ plane with subdivisions in meters of 0.05 by 0.05.

The changes in pressure over the hull are presented in figure 14 and 15. Here the pressure coefficient C_p in a front view of the hull model is exposed. Breaking wave is also showed in those figures. Figure 14 represents FAO1 (left) and FAO1b (right) while figure 15 shows FAO2 (left) and FAO2b (right). For both cases, it is appreciated that the pressure distribution changes once the bow is used. The high pressure area is smaller for FAO1b and FAO2b what is traduced in less pressure forces. Although those charts are taken in an instant time step, the breaking wave behaviour is close to the one obtained experimentally, see figure 16. In this figure, it is appreciated that the use of polyhedral bow smooths the diffracted wave and the flow over the model for v= 1.8 m/s.

6. Conclusions

In this work, the hydrodynamic influence of a dihedral bows on small fishing vessels is evaluated numerically. Certain small fishing vessels operate with a non optimized lines what consequently affects their operation efficiency. The purpose of this work was to provide

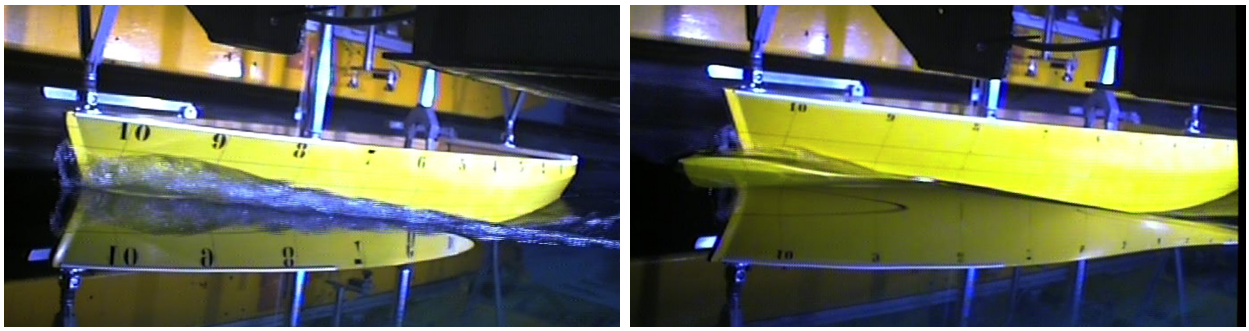

Figure 16: Towing tank photo at 1.8 m/s for: FAO1 left and FAO1b right

detailed information about the improvement in resistance produced when dihedral bulbous bows are used in those small fishing vessels.

Drawing lines provided by a FAO database were used for the dihedral bow implementation, and a later resistance comparison between the original model and the proposed one was made. Based on presented the work, Pérez-Arribas et al. (2022), where a description of the way this bulbous is designed and implemented in small fishing vessels, two hull shapes were selected for the actual work, a displacement hull and a semi - displacement hull.

Firstly, towing tank experiments were carried out pointing out the large reduction of resistance when the dihedral bow is implemented and tested in calm water. Due to the necessity of understanding why this change is produced, CFD simulations are run with the numerical tool OpenFOAM. CFDs allows the possibility of presenting a force decomposition, viscous resistance [R_v] and pressure force [R_p], together with pressure and wave distributions. The CFD analysis in calm water produces the following main conclusions:

- The use of dihedral bows is more efficient in displacement models in comparison with semi displacement-models. This is due to that the changes produced by the bow in the pressure force that present higher values in displacement ships.

- Dihedral bows have no relevant influence in viscous force. The changes in R_v for all the cases evaluated are not relevant enough when a dihedral bow is used. Besides, the major contribution to the total resistance comes from the R_p, therefore minor changes in R_v does not produce significant changes in the total resistance except for v 1.8 m/s

and displacement hull.

- As introduced in the precious item. R_p is the proportion of resistance more relevant for this research. This resistance becomes more relevant for high velocities since it tends to grow linearly and sometimes exponentially. Because the dihedral bow is altering the pressure field and therefore reducing the pressure force, if the speed of the model increased, the dihedral bow works better producing a better optimization of the total.

- Comparing conventional submerged bulbous bows with the dihedral bows, the last one do not affect significantly the radiated wave pattern.

- CFD shows enough precision at design speed to be used alone in future research and design.

Although this dihedral bow should be evaluated in other types of ship, waves and in other loading conditions, in this paper is proven that this design changes the pressure resistance and it is highly recommended for the tested fishing vessels because the total resistance is reduced.

Acknowledgements

Juan Luis Chacón from ETSIN Model Basin, who was the key person in the experimental tests. Thanks to Adriana Oliva to Amadeo Morán who worked initially in the calculations. This work was initially supported by the Spanish Ministerio de Economía y Competitividad through research grant TRA2015-67788-P and partially supported by ACIISI-Gobierno de Canarias and European FEDER Funds Grant EIS 2021 04.

References

Campana, E., D. Peri, Y. Tahara, and F. Stern (2006, 12). Shape optimization in ship hydrodynamics using computational fluid dynamics. *Computer Methods in Applied Mechanics and Engineering 196*, 634–651.

Díaz-Ojeda, H. R., F. J. Huera-Huarte, and L. M. González-Gutiérrez (2019). Hydrodynamics of a rigid stationary flat plate in cross-flow near the free surface. *Physics of Fluids 31*(10), 102108.

FVDD (2021). Fishing vessel design database (fvdd) 2021. *https://www.fao.org/fishery/en/vesseldesign/search*.

Guldhammer and Harvard (1974). Ship resistance.

Holtrop, J. and G. Mennen (1982). An approximate power prediction method. *International shipbuilding progress 29*, 166–170.

Huang, F. and C. Yang (2016). Hull form optimization of a cargo ship for reduced drag. *Journal of Hydrodynamics, Ser. B 28*(2), 173–183.

Islam, H. and C. Guedes Soares (2019). Uncertainty analysis in ship resistance prediction using openfoam. *Ocean Engineering 191*, 105805.

Issa, R. (1986). Solution of the implicitly discretised fluid flow equations by operator-splitting. *Journal of Computational Physics 62*(1), 40–65.

ITTC (2008). Recommended procedures and guidelines. procedure. uncertainty analysis in cfd verification and validation,. methodology and procedures.

ITTC (2011). Recommended procedures and guidelines. practical guidelines for ship cfd applications.

ITTC (2014). Recommended procedures and guidelines. practical guidelines for ship cfd applications.

ITTC (2017a). Recommended procedure guidelines: Resistance and propulsion tests and performance prediction with skinfriction drag reduction techniques.

ITTC (2017b). Recommended procedures and guidelines. procedure. uncertainty analysis in cfd verification and validation,. methodology and procedures.

ITTC (2021). The specialist committee on cfd and efd combined methods final report and recommendations to the 29 th ittc.

Jasak, H., A. Jemcov, and Z. Tukovic (2013, 11). Openfoam: A c++ library for complex physics simulations.

Jasak, H., V. Vukcevic, I. Gatin, and I. Lalovic (2019). Cfd validation and grid sensitivity studies of full scale ship self propulsion. *International Journal of Naval Architecture and Ocean Engineering 11*(1), 33–43.

Kim, H. and C. Yang (2010). A new surface modification approach for cfd-based hull form optimization. *Journal of Hydrodynamics, Ser. B 22*(5, Supplement 1), 520–525.

Korican, M., M. PerciÄ‡, N. Vladimir, N. AlujeviÄ‡, and A. Fan (2022). Alternative power options for improvement of the environmental friendliness of fishing trawlers. *Journal of Marine Science and Engineering 10*(12).

Larsson, L., F. Stern, M. Visonneau, T. Hino, N. Hirata, and J. Kim (2015). Proceedings, tokyo 2015 workshop on cfd in ship hydrodynamics.

Liu, X., W. Zhao, and D. Wan (2021). Hull form optimization based on calm-water wave drag with or without generating bulbous bow. *Applied Ocean Research 116*, 102861.

Menter, F. *Zonal Two Equation k-w Turbulence Models For Aerodynamic Flows.*

Menter, F., M. Kuntz, and R. Langtry (2003, January). Ten years of industrial experience with the sst turbulence model. *Heat and Mass Transfer 4*.

Menter, F. R. (1994). Two-equation eddy-viscosity turbulence models for engineering applications. *AIAA Journal 32*(8), 1598–1605.

Molland, A. F., S. R. Turnock, and D. A. Hudson (2017). *Ship Resistance and Propulsion: Practical Estimation of Ship Propulsive Power* (2 ed.). Cambridge University Press.

Moukalled, F., L. Mangani, and M. Darwish (2015). *The Finite Volume Method in Computational Fluid Dynamics: An Advanced Introduction with OpenFOAM and Matlab* (1st ed.). Springer Publishing Company, Incorporated.

Nazemian, A. and P. Ghadimi (2021). Cfd-based optimization of a displacement trimaran hull for improving its calm water and wavy condition resistance. *Applied Ocean Research 113*, 102729.

Niklas, K. and H. Pruszko (2019). Full-scale cfd simulations for the determination of ship resistance as a rational, alternative method to towing tank experiments. *Ocean Engineering 190*, 106435.

OpenFOAM. https://openfoam.org/.

Oro, J. (2012). *Técnicas numéricas en ingeniería de fluidos: Introducción a la dinámica de fluidos computacional (CFD) por el método de volúmenes finitos*. Editorial Reverte.

Pena, B. and L. Huang (2021). A review on the turbulence modelling strategy for ship hydrodynamic simulations. *Ocean Engineering 241*, 110082.

Percival, S., D. Hendrix, and F. Noblesse (2001). Hydrodynamic optimization of ship hull forms. *Applied Ocean Research 23*(6), 337–355.

Pérez-Arribas, F., A. Silva-Campillo, and H. R. Díaz-Ojeda (2022). Design of dihedral bows: A new type of developable added bulbous bows—experimental results. *Journal of Marine Science and Engineering 10*(11).

Rabaud, M. and F. Moisy (2013, May). Ship wakes: Kelvin or mach angle? *Phys. Rev. Lett. 110*, 214503.

SST-Model. https://www.openfoam.com/documentation/guides/latest/doc/guide-turbulence-ras-k-omega-sst.html.

Sugianto, E., J.-H. Chen, and N. V. A. Permadi (2022). Effect of monohull type and catamaran hull type on ocean waste collection behavior using openfoam. *Water 14*(17).

Szelangiewicz, T., T. Abramowski, K. Zelazny, and K. Sugalski (2021). Reduction of resistance, fuel consumption and ghg emission of a small fishing vessel by adding a bulbous bow. *Energies 14*(7).

Versteeg, H. and W. Malalasekera (2007). *An Introduction to Computational Fluid Dynamics: The Finite Volume Method*. Pearson Education Limited.

Voxakis, P. (2012). *Ship hull resistance calculations using CFD methods*. Ph. D. thesis, Massachusetts Institute of Technology, Dept. of Mechanical Engineering.

Xu, L. and Y. Wang (2001). - the fine optimization of ship hull lines in resistance performance by using cfd approach. In Y.-S. Wu, W.-C. Cui, and G.-J. Zhou (Eds.), *Practical Design of Ships and Other Floating*

Structures, pp. 59–65. Oxford: Elsevier Science Ltd.

Yanuar and K. T. Waskito (2017). Experimental study of total hull resistance of pentamaran ship model with varying configuration of outer side hulls. *Procedia Engineering 194*, 104–111. 10th International Conference on Marine Technology, MARTEC 2016.

Zha, L., R. Zhu, L. Hong, and S. Huang (2021). Hull form optimization for reduced calm-water resistance and improved vertical motion performance in irregular head waves. *Ocean Engineering 233*, 109208.